Review

Saturation overshoot and hysteresis for twophase flow in porous media[*]

R. Hilfer and R. Steinle

Institute for Computational Physics, Universität Stuttgart, 70569 Stuttgart, Germany

Abstract. Saturation overshoot and hysteresis for two phase flow in porous media are briefly reviewed. Old and new challenges are discussed. It is widely accepted that the traditional Richards model for twophase flow in porous media does not support non-monotone travelling wave solutions for the saturation profile. As a concequence various extensions and generalizations have been recently discussed. The review highlights different limits within the traditional theory. It emphasizes the relevance of hysteresis in the Buckley–Leverett limit with jump-type hysteresis in the relative permeabilities. Reviewing the situation it emerges that the traditional theory may have been abandoned prematurely because of its inability to predict saturation overshoot in the Richards limit.

1 Introduction for non-specialists

A macroscopic theory of two phase flow inside a rigid porous medium poses not only challenges to nonequilibrium statistical physics and geometry [1], but is also crucial for many applications [1–10]. Despite its popularity, the accepted macroscopic theory of two phase flow seems unable to reproduce the experimentally observed phenomenon of saturation overshoot [11].

Models for twophase flow in porous media can be divided into macroscopic (laboratory or field scale) models popular in engineering, and microscopic (pore scale) models such as network models [12–17] that are popular in physics. As of today no rigorous connection exists between microscopic and macroscopic models [1,18]. In view of the predominantly non-specialist readership with a physics background, it is appropriate to remind the reader of the traditional theory, introduced between 1907 and 1941 by Buckingham, Richards, Muskat, Meres, Wyckoff, Botset, Leverett and others [19–23][1]. One formulation of the traditional macroscopic theory starts from the fundamental balance laws of continuum mechanics for two fluids (called water $\mathbb{W}$ and oil $\mathbb{O}$) inside the pore space (called $\mathbb{P}$) of a porous sample $\mathbb{S} = \mathbb{P} \cup \mathbb{M}$ with a rigid

---

[*] Ideas and partial results were discussed at the NUPUS-Workshop on "Saturation overshoot, dynamic capillary pressure and production term", September 27th–28th, 2013, Stuttgart, Germany.

[1] The following introductory paragraphs are quoted from [24] for convenience of the interdisciplinary readership and following an explicit request from the editor.

solid matrix (called $\mathbb{M}$). Recall the law of mass balance in differential form

$$\frac{\partial(\phi_i \varrho_i)}{\partial t} + \nabla \cdot (\phi_i \varrho_i \mathbf{v}_i) = M_i \tag{1}$$

where $\varrho_i(\mathbf{x}, t), \phi_i(\mathbf{x}, t), \mathbf{v}_i(\mathbf{x}, t)$ denote mass density, volume fraction and velocity of phase $i = \mathbb{W}, \mathbb{O}$ as functions of position $\mathbf{x} \in \mathbb{S} \subset \mathbb{R}^3$ and time $t \in \mathbb{R}_+$. Exchange of mass between the two phases is described by mass transfer rates M_i giving the amount of mass by which phase i changes per unit time and volume. Momentum balance for the two fluids requires in addition

$$\phi_i \varrho_i \frac{\mathrm{D}^i}{\mathrm{D}t} \mathbf{v}_i - \phi_i \nabla \cdot \Sigma_i - \phi_i \mathbf{F}_i = \mathbf{m}_i - \mathbf{v}_i M_i \tag{2}$$

where Σ_i is the stress tensor in the ith phase, $\mathbf{F}_i$ is the body force per unit volume acting on the ith phase, $\mathbf{m}_i$ is the momentum transfer into phase i from all the other phases, and $\mathrm{D}^i/\mathrm{D}t = \partial/\partial t + \mathbf{v}_i \cdot \nabla$ denotes the material derivative for phase $i = \mathbb{W}, \mathbb{O}$.

Defining the saturations $S_i(\mathbf{x}, t)$ as the volume fraction of pore space $\mathbb{P}$ filled with phase i one has the relation $\phi_i = \phi S_i$ where ϕ is the porosity of the sample. Expressing volume conservation $\phi_{\mathbb{W}} + \phi_{\mathbb{O}} = \phi$ in terms of saturations yields

$$S_{\mathbb{W}} + S_{\mathbb{O}} = 1. \tag{3}$$

In order to obtain the traditional theory, these balance laws for mass, momentum and volume have to be combined with specific constitutive assumptions for $M_i, \mathbf{m}_i, \mathbf{F}_i$ and Σ_i.

Great simplification is afforded by assuming that the porous medium is rigid and macroscopically homogeneous

$$\phi(\mathbf{x}, t) = \phi = \text{const} \tag{4}$$

although this is often violated in applications [25]. Let us focus first on the momentum balance (2). One assumes that the stress tensor of the fluids is diagonal

$$\Sigma_{\mathbb{W}} = -P_{\mathbb{W}} \mathbf{1} \tag{5a}$$
$$\Sigma_{\mathbb{O}} = -P_{\mathbb{O}} \mathbf{1} \tag{5b}$$

where $P_{\mathbb{W}}, P_{\mathbb{O}}$ are the fluid pressures. Realistic subsurface flows have low Reynolds numbers so that the inertial term

$$\frac{\mathrm{D}^i}{\mathrm{D}t} \mathbf{v}_i = 0 \tag{6}$$

can be neglected in the momentum balance Eq. (2). It is further assumed that the body forces

$$\mathbf{F}_{\mathbb{W}} = -\varrho_{\mathbb{W}} g \mathbf{e}_z \tag{7a}$$
$$\mathbf{F}_{\mathbb{O}} = -\varrho_{\mathbb{O}} g \mathbf{e}_z \tag{7b}$$

are given by gravity. As long as there are no chemical reactions between the fluids the mass transfer rates vanish, so that $M_{\mathbb{W}} = -M_{\mathbb{O}} = 0$ holds. Momentum transfer between the fluids and the rigid matrix is dominated by viscous drag in the form

$$\mathbf{m}_{\mathbb{W}} = -k^{-1} \frac{\mu_{\mathbb{W}} \phi_{\mathbb{W}}^2}{k_{\mathbb{W}}^r(S_{\mathbb{W}})} \mathbf{v}_{\mathbb{W}} \tag{8a}$$

$$\mathbf{m}_{\mathbb{O}} = -k^{-1} \frac{\mu_{\mathbb{O}} \phi_{\mathbb{O}}^2}{k_{\mathbb{O}}^r(S_{\mathbb{W}})} \mathbf{v}_{\mathbb{O}} \tag{8b}$$

where $\mu_{\mathbb{W}}, \mu_{\mathbb{O}}$ are the constant fluid viscosities, k is the absolute permeability tensor, and $k_{\mathbb{W}}^r(S_{\mathbb{W}}), k_{\mathbb{O}}^r(S_{\mathbb{W}})$ are the nonlinear relative permeabilitiy functions for water and oil [2].

Inserting the constitutive assumptions (4)–(8) into the mass balance Eq. (1) yields

$$\frac{\partial(\varrho_{\mathbb{W}} S_{\mathbb{W}})}{\partial t} + \nabla \cdot (\varrho_{\mathbb{W}} S_{\mathbb{W}} \mathbf{v}_{\mathbb{W}}) = 0 \tag{9a}$$

$$\frac{\partial(\varrho_{\mathbb{O}} S_{\mathbb{O}})}{\partial t} + \nabla \cdot (\varrho_{\mathbb{O}} S_{\mathbb{O}} \mathbf{v}_{\mathbb{O}}) = 0 \tag{9b}$$

while the momentum balance Eq. (2)

$$\phi_{\mathbb{W}} \mathbf{v}_{\mathbb{W}} = -\frac{k}{\mu_{\mathbb{W}}} k_{\mathbb{W}}^r(S_{\mathbb{W}})(\nabla P_{\mathbb{W}} - \varrho_{\mathbb{W}} g \mathbf{e}_z) \tag{10a}$$

$$\phi_{\mathbb{O}} \mathbf{v}_{\mathbb{O}} = -\frac{k}{\mu_{\mathbb{O}}} k_{\mathbb{O}}^r(S_{\mathbb{W}})(\nabla P_{\mathbb{O}} - \varrho_{\mathbb{O}} g \mathbf{e}_z) \tag{10b}$$

give the generalized Darcy laws for the Darcy velocities $\phi_i \mathbf{v}_i$ [3, p. 155]. Equations (9) and (10) together with Eq. (3) provide 9 equations for 12 primary unknowns $S_{\mathbb{W}}, S_{\mathbb{O}}, \varrho_{\mathbb{W}}, \varrho_{\mathbb{O}}, P_{\mathbb{W}}, P_{\mathbb{O}}, \mathbf{v}_{\mathbb{W}}, \mathbf{v}_{\mathbb{O}}$. Additional equations are needed.

Observations of capillary rise in regular packings [26] suggest that the pressure difference between oil and water in general should depend only on saturation [23]

$$P_{\mathbb{O}} - P_{\mathbb{W}} = \sigma_{\mathbb{W}\mathbb{O}} \kappa(S_{\mathbb{W}}) = P_c(S_{\mathbb{W}}) \tag{11}$$

where $\sigma_{\mathbb{W}\mathbb{O}}$ is the oil–water interfacial tension and $\kappa(S_{\mathbb{W}})$ is the mean curvature of the oil–water interface. The system of equations is closed with two equations of state relating the phase pressures and densities. In petroleum engineering the two fluids are usually assumed to be incompressible

$$\varrho_{\mathbb{W}}(\mathbf{x}, t) = \varrho_{\mathbb{W}} = \text{const} \tag{12a}$$

$$\varrho_{\mathbb{O}}(\mathbf{x}, t) = \varrho_{\mathbb{O}} = \text{const} \tag{12b}$$

while in hydrology one thinks of water $\mathbb{W}$ and air $\mathbb{O}$ setting

$$\varrho_{\mathbb{W}}(\mathbf{x}, t) = \varrho_{\mathbb{W}} = \text{const} \tag{12c}$$

$$\varrho_{\mathbb{O}}(\mathbf{x}, t) = \frac{P_{\mathbb{O}}(\mathbf{x}, t)}{R_s T} \tag{12d}$$

where $R_s \approx 287\text{J kg}^{-1}\text{K}^{-1}$ is the specific gas constant and the temperature T is assumed to be constant throughout $\mathbb{S}$.

When the fluids (water and oil) are incompressible (as in petroleum engineering) Eqs. (12a) and (12b) hold. In this case, adding Eqs. (9a) and (9b), using Eq. (3) and integrating the result shows

$$\mathbf{q}_{\mathbb{W}}(\mathbf{x}, t) + \mathbf{q}_{\mathbb{O}}(\mathbf{x}, t) = \mathbf{Q}(t) \tag{13}$$

where the total volume flux $\mathbf{Q}$ is independent of $\mathbf{x}$ and $\mathbf{q}_i = \phi_i \mathbf{v}_i = \phi S_i \mathbf{v}_i$ with $i = \mathbb{W}, \mathbb{O}$ are the volume flux of water and oil. Inserting Eqs. (10) into Eq. (13) and using Eq. (11) to eliminate $P_{\mathbb{W}}$ gives

$$\mathbf{Q} = -k\lambda \left[\nabla P_{\mathbb{O}} - f_{\mathbb{W}} \nabla P_c - (f_{\mathbb{W}} \varrho_{\mathbb{W}} + f_{\mathbb{O}} \varrho_{\mathbb{O}}) g \mathbf{e}_z \right] \tag{14}$$

---

[2] $k_{\mathbb{W}}^r(S_{\mathbb{W}}), k_{\mathbb{O}}^r(S_{\mathbb{W}})$ account for the fact, that the experimentally observed permability of two immiscible fluids deviates from their partial (or mean field) permeabilities $kS_{\mathbb{W}}, kS_{\mathbb{O}}$ obtained from volume averaging of the absolute permeability.

where (with $i = \mathbb{W}, \mathbb{O}$)

$$\lambda_i = \frac{k_i^r}{\mu_i}; \qquad \lambda = \lambda_\mathbb{W} + \lambda_\mathbb{O}; \qquad f_i = \frac{\lambda_i}{\lambda} \tag{15}$$

are the mobilities λ_i, total mobility λ and fractional flow functions f_i, respectively. Multiplying Eq. (10a) with $f_\mathbb{O}$, Eq. (10b) with $f_\mathbb{W}$ and subtracting Eq. (10b) from Eq. (10a), using Eq. (13) and $f_\mathbb{W} + f_\mathbb{O} = 1$ to eliminate $\mathbf{q}_\mathbb{O}$ gives the result

$$\mathbf{q}_\mathbb{W} = f_\mathbb{W} \left[\mathbf{Q} + k\lambda_\mathbb{O}(\varrho_\mathbb{W} - \varrho_\mathbb{O})g\mathbf{e}_z \right] + k\frac{\lambda_\mathbb{W}\lambda_\mathbb{O}}{\lambda}\nabla P_\mathrm{c} \tag{16}$$

which can be inserted into Eq. (9a) to give

$$\phi\frac{\partial S_\mathbb{W}}{\partial t} + \nabla \cdot \left\{ f_\mathbb{W}(S_\mathbb{W})\left[\mathbf{Q} + k\lambda_\mathbb{O}(S_\mathbb{W})(\varrho_\mathbb{W} - \varrho_\mathbb{O})g\mathbf{e}_z + k\lambda_\mathbb{O}(S_\mathbb{W})\nabla P_\mathrm{c}(S_\mathbb{W})\right] \right\} = 0 \tag{17}$$

a nonlinear partial differential equation for the saturation field $S_\mathbb{W}(\mathbf{x}, t)$. For small k or when gravity and capillarity effects can be neglected the last two terms vanish and Eq. (17) reduces to the Buckley–Leverett equation [27]

$$\phi\frac{\partial S_\mathbb{W}}{\partial t} + \mathbf{Q} \cdot \nabla f_\mathbb{W}(S_\mathbb{W}) = 0 \tag{18}$$

a quasilinear hyperbolic partial differential equation. Equation (17) supplemented with a (quasilinear elliptic) equation obtained from $\nabla \cdot \mathbf{Q} = 0$ by defining a global pressure in such a way that the total flux $\mathbf{Q}$ obeys a Darcy law with respect to the global pressure provides, for incompressible fluids, an equivalent formulation of Eqs. (9)–(12b). For compressible fluids the situation is different.

When $\mathbb{W}$ corresponds to water and $\mathbb{O}$ to air (as for applications in hydrology) Eqs. (12c) and (12d) hold. The large density difference $\varrho_\mathbb{O} \ll \varrho_\mathbb{W}$ suggests to consider the case $\varrho_\mathbb{O} \approx 0$ of a very rarified gas or vacuum as a first approximation. For $\varrho_\mathbb{O} = 0$ Eq. (9b) is identically fulfilled, Eq. (12d) implies $P_\mathbb{O} = 0$ and then Eq. (10b) implies $\mathbf{v}_\mathbb{O} = 0$. In this way the $\mathbb{O}$-phase vanishes from the problem and one is left only with the $\mathbb{W}$-phase. Inserting Eq. (10a) into Eq. (9a) and using Eq. (11) gives the Richards equation [20]

$$\phi\frac{\partial S_\mathbb{W}}{\partial t} + \nabla \cdot \left\{ k\,\lambda_\mathbb{W}(S_\mathbb{W})\left[\nabla P_\mathrm{c}(S_\mathbb{W}) + \varrho_\mathbb{W} g\mathbf{e}_z\right] \right\} = 0 \tag{19a}$$

for saturation or

$$\phi\frac{\partial \theta(P_\mathbb{W})}{\partial t} = \nabla \cdot \left[k\,\lambda_\mathbb{W}(\theta(P_\mathbb{W}))\left\{\nabla P_\mathbb{W} - \varrho_\mathbb{W} g\mathbf{e}_z\right\} \right] \tag{19b}$$

for pressure after writing $S_\mathbb{W}(\mathbf{x}, t) = P_\mathrm{c}^{-1}(-P_\mathbb{W}(\mathbf{x}, t)) = \theta(P_\mathbb{W}(\mathbf{x}, t))$ with the help of Eq.(11). To define the nonlinear function $\theta(P_\mathbb{W})$ the typical sigmoidal shape has been assumed for $P_\mathrm{c}(x)$.

The quasilinear elliptic–parabolic Richards Eq. (19) is the basic equation in hydrology, while the quasilinear hyperbolic Buckley–Leverett Eq. (18) is fundamental for applications in petroleum engineering. Both Eqs. (18) and (19), differ from the general fractional flow formulation (17) in terms of saturation $S_\mathbb{W}$ and global pressure P. They differ also from the formulation in terms of $S_\mathbb{W}, S_\mathbb{O}, \mathbf{v}_\mathbb{W}, \mathbf{v}_\mathbb{O}, P_\mathbb{W}, P_\mathbb{O}$ given by (3), (9), (10) and (11). These latter equations appropriately supplemented with initial and boundary conditions and spaces of functions resp. generalized functions for the unknowns constitute the traditional theory of macroscopic capillarity in porous media.

The question of domains is important for wellposedness and numerical solution. For Eq. (18) it is well known that classical solutions, i.e. locally Lipschitz continuous functions, in general will exist only for a finite length of time [28–30]. Hence, it is necessary to consider also weak solutions [31]. Weak solutions are locally bounded, measurable functions satisfying Eq. (18) in the sense of distributions. Weak solutions are frequently constructed by the method of vanishing viscosity or the theory of contraction semigroups. For the Richards Eq. (19) a domain of definition in the space of Bochner-square-integrable Sololev-space-valued functions has been discussed in [32]. In many engineering applications formulations such as Eqs. (17), (18) or (19) with (11) augmented with appropriate initial and boundary conditions are solved by computer programs [33–35]. This concludes our brief introduction into the traditional theory.

2 Open questions

Numerous open questions surround the traditional model above. Important examples are the macroscopic effects of capillarity and surface tensions, the spatiotemporal variability of residual saturations, hysteresis and saturation overshoot (see e.g. [1, 18,24,36–50] and references therein). In this paper, we focus on the interplay and relation between hysteresis and saturation overshoot.

Saturation overshoot refers to the experimental observation of non-monotone saturation profiles during certain classes of infiltration problems, where fingers of infiltrating water develop due to gravitational instabilities [51–55]. Within the fingers, the profile of water saturation is non-monotone [53]. Experiments in relatively thin tubes, with diameter less than the characteristic finger width, show the existence of similar non-monotone profiles [53–55].

Many theoretical and numerical investigations in recent years have addressed saturation overshoot and gravity driven fingering and their relation to each other [11,56–66]. Reference [56] reported saturation overshoot in numerical solutions of Richards equation when the hydraulic conductivities between collocation points weighted appropriately in the numerical scheme. In [11] it was argued that these overshoot solutions are numerical artifacts generated by truncation errors. This finding agreed with earlier mathematical proofs of existence, uniqueness and stability of solutions within a L^1-theory for a class of quasilinear elliptic–parabolic equations [32,57,58,67]. These were applied to the Richards equation [32,61,68] leading to the conclusion that the conventional theory is inadequate to represent fingering and overshoot [61,63,68–70].

Accordingly, new approaches were proposed [48,60,63–65,71,72]. Reference [60] discussed additional terms in Richards equation, meant to represent a so called hold-back-pile-up effect. Other suggestions are based on dynamic extensions of capillary pressure [63,71,72]. Some authors proposed an additional term based on the yet to be observed "effective macroscopic surface tension" [64,65]. Saturation overshoot profiles at rest when the velocities of all fluids vanish were recently predicted within an approach based on distinguishing percolating and nonpercolating (trapped, immobile) fluid parts in [48].

The overshoot phenomenon continues to challenge researchers in the field. There is an ongoing and lively scientific debate on the subject as witnessed by numerous publications (see also [70] for more references). Very recently, DiCarlo and coworkers [69] investigated the physics behind the displacement front using the traditional model of two phase flow. They argue that gas is drawn in behind the overshoot tip and that the viscosity of this gas plays an observable role when the infiltrating flux is large. They emphasize, however, that in their paper they are *"not concerned with why the overshoot occurs, or in other words why the saturation jumps"* and that *"adding in*

the viscosity of the displaced phase...,does not change the arguments" of van Duijn *et al.* [63]. According to these arguments the traditional standard model leads to parabolic equations and hence overshoot behaviour is not allowed [69, p. 965].

The objective for the rest of this paper is to review analytical and numerical evidence for the possible existence of non-monotone solutions (saturation overshoot profiles) within the traditional standard theory outlined above.

3 Saturation overshoot

3.1 Experimental observations

Infiltration experiments [59] on constant flux imbibition into a very dry porous medium report existence of non-monotone travelling wave profiles for the saturation [55, 62]

$$S(z,t) = s(y) \tag{20}$$

as a function of time $t \geq 0$ and position $0 \leq z \leq 1$ along the column. Here $-\infty < y < \infty$ denotes the similarity variable

$$y = z - c^* t \tag{21}$$

and the parameter $-\infty < c^* < \infty$ is the constant wave velocity. From here on all quantitites z, t, y, S, c^* are dimensionless. The relation

$$\widehat{z} = zL \tag{22a}$$

defines the dimensional depth coordinate $0 \leq \widehat{z} \leq L$ increasing along the orientation of gravity. The length L is the system size (length of column). The dimensional time is

$$\widehat{t} = \frac{tL}{Q} \tag{22b}$$

where Q denotes the total (i.e. wetting plus nonwetting) spatially constant flux through the column in m/s (see Eq. (13)). The dimensional similarity variable reads

$$\widehat{y} = yL = \widehat{z} - c^* Q \widehat{t}. \tag{22c}$$

Experimental observations show fluctuating profiles with an overshoot region [54, 55, 59, 73–75]. It can be viewed as a travelling wave profile consisting of an imbibition front followed by a drainage front.

3.2 Mathematical formulation in $d = 1$

The problem is to determine the height S^* of the overshoot region (=tip) and its velocity c^* given an initial profile $S(z, 0)$, the outlet saturation S^{out}, and the saturation S^{in} at the inlet as data of the problem. Constant Q and constant S^{in} are assumed for the boundary conditions at the left boundary. Note, that this differs from the experiment, where the flux of the wetting phase and the pressure of the nonwetting phase are controlled.

The leading (imbibition) front is a solution of the nondimensionalized fractional flow equation (obtained from Eq. (17) for $d = 1$)

$$\phi \frac{\partial S}{\partial t} + \frac{\partial}{\partial z} \left[f_{\text{im}}(S) - D_{\text{im}}(S) \frac{\partial S}{\partial z} \right] = 0 \tag{23a}$$

while

$$\phi \frac{\partial S}{\partial t} + \frac{\partial}{\partial z}\left[f_{\mathrm{dr}}(S) - D_{\mathrm{dr}}(S)\frac{\partial S}{\partial z}\right] = 0 \tag{23b}$$

must be fulfilled at the trailing (drainage) front. Here ϕ is the porosity and the variables z and t have been nondimensionalized using the system size L and the total flux Q. The latter is assumed to be constant. The functions $f_{\mathrm{im}}, f_{\mathrm{dr}}$ are the fractional flow functions for primary imbibition and secondary drainage. They are given as

$$f_i(S) = \frac{\dfrac{\mu_{\mathbb{O}}}{\mu_{\mathbb{W}}}\dfrac{k^r_{\mathbb{W}_i}(S)}{k^r_{\mathbb{O}_i}(S)} + \dfrac{k^r_{\mathbb{W}_i}(S)}{\mathrm{Gr}_{\mathbb{W}}}\left(1 - \dfrac{\varrho_{\mathbb{O}}}{\varrho_{\mathbb{W}}}\right)}{1 + \dfrac{\mu_{\mathbb{O}}}{\mu_{\mathbb{W}}}\dfrac{k^r_{\mathbb{W}_i}(S)}{k^r_{\mathbb{O}_i}(S)}} \tag{24a}$$

$$= \frac{1 + \dfrac{k^r_{\mathbb{O}_i}(S)}{\mathrm{Gr}_{\mathbb{W}}}\dfrac{\mu_{\mathbb{W}}}{\mu_{\mathbb{O}}}\left(1 - \dfrac{\varrho_{\mathbb{O}}}{\varrho_{\mathbb{W}}}\right)}{1 + \dfrac{\mu_{\mathbb{W}}}{\mu_{\mathbb{O}}}\dfrac{k^r_{\mathbb{O}_i}(S)}{k^r_{\mathbb{W}_i}(S)}} \tag{24b}$$

with $i \in \{\mathrm{im}, \mathrm{dr}\}$ and the dimensionless gravity number [37,76]

$$\mathrm{Gr}_{\mathbb{W}} = \frac{\mu_{\mathbb{W}}Q}{\varrho_{\mathbb{W}}gk} \tag{25}$$

defined in terms of total flux Q, wetting viscosity $\mu_{\mathbb{W}}$, density $\varrho_{\mathbb{W}}$, acceleration of gravity g and absolute permeability k of the medium. The functions $k^r_{\mathbb{W}_i}(S), k^r_{\mathbb{O}_i}(S)$ with $i \in \{\mathrm{im}, \mathrm{dr}\}$ are the relative permeabilities. The capillary flux functions for drainage and imbibition are defined as

$$D_i(S) = -\frac{\dfrac{k^r_{\mathbb{W}_i}(S)}{\mathrm{Ca}_{\mathbb{W}}}\dfrac{\mathrm{d}P_{c_i}(S)}{\mathrm{d}S}}{1 + \dfrac{\mu_{\mathbb{O}}}{\mu_{\mathbb{W}}}\dfrac{k^r_{\mathbb{W}_i}(S)}{k^r_{\mathbb{O}_i}(S)}} \tag{26}$$

with $i \in \{\mathrm{im}, \mathrm{dr}\}$ and a minus sign was introduced to make them positive. The functions P_{c_i} are capillary pressure saturation relations for drainage and imbibition. The dimensionless number

$$\mathrm{Ca}_{\mathbb{W}} = \frac{\mu_{\mathbb{W}}QL}{P_{\mathrm{b}}k} \tag{27}$$

is the macroscopic capillary number [37,76] with P_{b} representing a typical (mean) capillary pressure at $S = 0.5$ (see Eq. (34)). For $\mathrm{Ca} = \infty$, one has $D_i = 0$ and Eqs. (23) reduce to two nondimensionalized Buckley–Leverett equations

$$\phi \frac{\partial S}{\partial t} + \frac{\partial}{\partial z}f_{\mathrm{im}}(S) = 0 \tag{28a}$$

for the leading (imbibition) front and

$$\phi \frac{\partial S}{\partial t} + \frac{\partial}{\partial z}f_{\mathrm{dr}}(S) = 0 \tag{28b}$$

for the trailing (drainage) front.

3.3 Hysteresis

Conventional hysteresis models for the traditional theory require to store the process history for each location inside the sample [77–79]. Usually this means to store the pressure and saturation history (i.e. the reversal points, where the process switches between drainage and imbibition). A simple jump-type hysteresis model can be formulated locally in time based on Eq. (23) as

$$
\phi \frac{\partial S}{\partial t} + \Xi(S) \frac{\partial}{\partial z} \left[f_{\mathrm{im}}(S) - D_{\mathrm{im}}(S) \frac{\partial S}{\partial z} \right]
$$
$$
+ \left[1 - \Xi(S) \right] \frac{\partial}{\partial z} \left[f_{\mathrm{dr}}(S) - D_{\mathrm{dr}}(S) \frac{\partial S}{\partial z} \right] = 0. \tag{29}
$$

Here $\Xi(S)$ denotes the left sided limit

$$
\Xi(S) = \lim_{\varepsilon \to 0} \Theta \left[\frac{\partial S}{\partial t}(z, t - \varepsilon) \right], \tag{30}
$$

$\Theta(x)$ is the Heaviside step function (see Eq. (35)), and the parameter functions $f_i(S), D_i(S)$ with $i \in \{\mathrm{dr}, \mathrm{im}\}$ require a pair of capillary pressure and two pairs of relative permeability functions as input. The relative permeability functions employed for computations are of van Genuchten form [80,81]

$$
k^r_{\mathbb{W}_i}(S_{e_i}) = K^e_{\mathbb{W}_i} S_{e_i}^{1/2} \left[1 - (1 - S_{e_i}^{1/\alpha_i})^{\alpha_i} \right]^2 \tag{31a}
$$

$$
k^r_{\mathbb{O}_i}(S_{e_i}) = K^e_{\mathbb{O}_i} (1 - S_{e_i})^{1/2} (1 - S_{e_i}^{1/\beta_i})^{2\beta_i} \tag{31b}
$$

with $i \in \{\mathrm{im}, \mathrm{dr}\}$ and

$$
S_{e_i}(S) = \frac{S - S_{\mathbb{W}i}{}^i}{1 - S_{\mathbb{O}r}{}^i - S_{\mathbb{W}i}{}^i} \tag{32}
$$

the effective saturation. The resulting fractional flow functions with parameters from Table 1 are shown in Fig. 1b. The capillary pressure functions used in the computations are

$$
P_{\mathrm{c}i}(S_{e_i}) = P_{\mathrm{b}i} \left(S_{e_i}^{-1/\alpha_i} - 1 \right)^{1-\alpha_i} \tag{33}
$$

with $i = \mathrm{dr}, \mathrm{im}$ and the typical pressure P_{b} in (27) is defined as

$$
P_{\mathrm{b}} = \frac{P_{\mathrm{cim}}(0.5) + P_{\mathrm{cdr}}(0.5)}{2}. \tag{34}
$$

Equation (29) with initial and boundary conditions for S and an initial condition for $\partial S/\partial t$ is conjectured to be a well defined semigroup of bounded operators on $L^1([0, L])$ on a finite interval $[0, T]$ of time. The conjecture is supported by the fact that each of the Eq. (23) individually defines such a semigroup, and because multiplication by Ξ or $(1 - \Xi)$ are projection operators.

4 Approximate analytical solution

4.1 Step function approximation

The basic idea of the analysis below is to approximate the travelling wave profile for long times $t \to \infty$ with piecewise constant functions (step functions). For large

$\mathrm{Ca} \to \infty$ (i.e. in the Buckley–Leverett limit) one may view this approximate profile as a superposition of two Buckley–Leverett shock fronts. This is possible by virtue of the fact, that the Heaviside step function

$$
\Theta(y) = \begin{cases} 1, & y > 0 \quad \text{or} \quad z/t > c^* \\[2mm] 0, & y \leq 0 \quad \text{or} \quad z/t \leq c^* \end{cases} \tag{35}
$$

can also be regarded as a function of the similarity variable z/t of the Buckley–Leverett problem.

In the crudest approximation one can split the total profile for sufficiently large t into the sum

$$
s(y) = s_{\mathrm{im}}(y) + s_{\mathrm{dr}}(y) \tag{36a}
$$

of an imbibition front

$$
s_{\mathrm{im}}(y) = S^{\mathrm{out}} + (S^{\mathrm{in}} - S^{\mathrm{out}}) \left[1 - \Theta(y - z^*) \right] \tag{36b}
$$

located at $z_{\mathrm{im}} = c^* t + z^*$ and a drainage front profile located at $z_{\mathrm{dr}} = c^* t$

$$
s_{\mathrm{dr}}(y) = (S^* - S^{\mathrm{in}}) \, \Theta(y) \left[1 - \Theta(y - z^*) \right] \tag{36c}
$$

both moving with the same speed c^*, where $S^{\mathrm{in}} = s(-\infty)$ resp. $S^{\mathrm{out}} = s(\infty)$ are the upper (inlet) resp. lower (outlet) saturations and S^* is the maximum (overshoot) saturation. The quantity $z^* = z_{\mathrm{im}} - z_{\mathrm{dr}}$ is the distance by which the imbibition front precedes the drainage front, i.e. the width of the tip (=overshoot) region.

4.2 Travelling wave solutions

The two Eq. (28) become coupled, if Eq. (20) holds true, because then there is only a single wave speed c^* for both fronts. At the imbibition discontinuity, the Rankine–Hugoniot condition demands

$$
c^* = \frac{f_{\mathrm{im}}(S^*) - f_{\mathrm{im}}(S^{\mathrm{out}})}{S^* - S^{\mathrm{out}}} := c_{\mathrm{im}}(S^*) \tag{37a}
$$

and the second equality (with colon) defines the function $c_{\mathrm{im}}(S)$. Similarly

$$
c^* = \frac{f_{\mathrm{dr}}(S^*) - f_{\mathrm{dr}}(S^{\mathrm{in}})}{S^* - S^{\mathrm{in}}} := c_{\mathrm{dr}}(S^*) \tag{37b}
$$

defines the drainage front velocity as a function $c_{\mathrm{dr}}(S)$ of the overshoot S^*. Examples of the velocities c_i used in the compuations are shown in Fig. 1a. For a travelling wave both fronts move with the same velocity so that the mathematical problem is to find a solution S^* of the equation

$$
c_{\mathrm{im}}(S^*) = c_{\mathrm{dr}}(S^*) \tag{38}
$$

obtained from equating Eqs. (37b) and (37a) (see Fig. 1a). The wave velocity c^* is then obtained as $c_{\mathrm{im}}(S^*)$ or equivalently as $c_{\mathrm{dr}}(S^*)$.
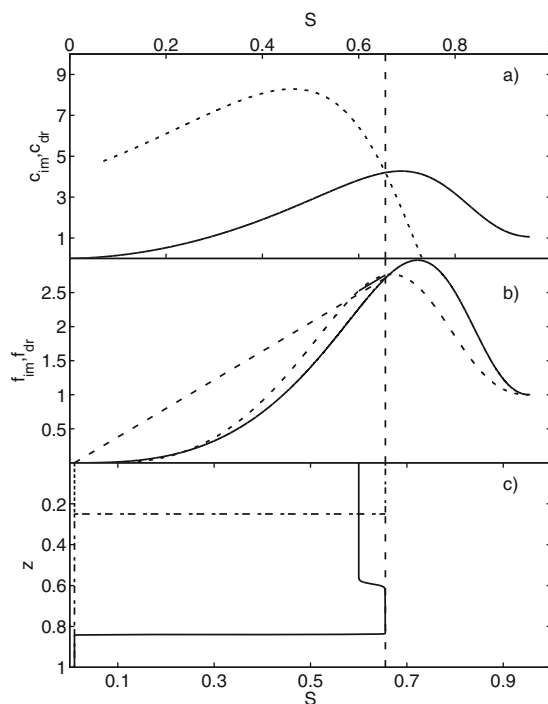
Fig. 1. a) Graphical solution of Eq. (38). The dashed curve shows $c_{dr}(S)$, the solid line shows $c_{im}(S)$. b) Fractional flow functions for drainage (dashed) and imbibition (solid). The two secants (solid/dashed) show the graphical construction of the travelling wave solution with $c_{im} = c_{dr} = c^*$. For better visibility, their line styles have been reversed. Their slopes are equal to each other. c) Numerical solution of eq. (29) using Open∇FOAM for the travelling wave constructed graphically in subfigure b). The solution is displayed at time $t = 0.053222$. The monotone initial profile at $t = 0$ is shown as a dash-dotted step.

4.3 General overshoot solutions with two wave speeds

Equation (38) provides a necessary condition for the existence of a travelling wave solution of the form of Eq. (36) with velocity c^* and overshoot S^*. More generally, if the saturation plateau S^{P} is larger or smaller than S^*, one expects to find non-monotone profiles that are, however, not travelling waves. Instead the drainage and imbibition fronts are expected to have different velocities. The fractional flow functions with relative permeabilities from Eq. (31) and the parameters from Table 1 give for $S^{\mathrm{P}} < S^*$ the result

$$c_{im}(S^{\mathrm{P}}) < c_{dr}(S^{\mathrm{P}}) \tag{39}$$

while for $S^{\mathrm{P}} > S^*$ one has

$$c_{im}(S^{\mathrm{P}}) > c_{dr}(S^{\mathrm{P}}). \tag{40}$$

In this case, for plateau saturations $S^{\mathrm{P}} < S^*$, the leading (imbibition) front has a smaller velocity than the trailing (drainage) front. Thus the trailing front catches up and the profile approaches a single front at long times. For plateau saturations $S^{\mathrm{P}} > S^*$ on the other hand the trailing drainage front moves slower than the leading imbibition front. In this case a non-monotone profile persists indefinitely, albeit with a plateau (tip) width that increases linearly with time.

Table 1. Parameter values, their symbols and units.

Parameter	Symbol	Value	Units
system size	L	1.0	m
porosity	ϕ	0.38	–
permeability	k	$2 \cdot 10^{-10}$	m^2
density $\mathbb{W}$	$\varrho_{\mathbb{W}}$	1000	kg/m^3
density $\mathbb{O}$	$\varrho_{\mathbb{O}}$	800	kg/m^3
viscosity $\mathbb{W}$	$\mu_{\mathbb{W}}$	0.001	Pa·s
viscosity $\mathbb{O}$	$\mu_{\mathbb{O}}$	0.0003	Pa·s
imbibition exp.	$\alpha_{\mathrm{im}} = \beta_{\mathrm{im}}$	0.85	–
drainage exp.	$\alpha_{\mathrm{dr}} = \beta_{\mathrm{dr}}$	0.98	–
end pnt. rel.p.	$K^e_{\mathbb{W}_{\mathrm{im}}}$	0.35	–
end pnt. rel.p.	$K^e_{\mathbb{O}_{\mathrm{im}}}$	1	–
end pnt. rel.p.	$K^e_{\mathbb{W}_{\mathrm{dr}}}$	0.35	–
end pnt. rel.p.	$K^e_{\mathbb{O}_{\mathrm{dr}}}$	0.75	–
imb. cap. press.	$P_{\mathrm{b}_{\mathrm{im}}}$	55.55	Pa
dr. cap. press.	$P_{\mathrm{b}_{\mathrm{dr}}}$	100	Pa
end pnt. sat.	$S_{\mathbb{W}\mathrm{i}}{}^{\mathrm{im}}$	0	–
end pnt. sat.	$S_{\mathbb{W}\mathrm{i}}{}^{\mathrm{dr}}$	0.07	–
end pnt. sat.	$S_{\mathbb{O}\mathrm{r}}{}^{\mathrm{im}}$	0.045	–
end pnt. sat.	$S_{\mathbb{O}\mathrm{r}}{}^{\mathrm{dr}}$	0.045	–
boundary sat.	S^{out}	0.01	–
boundary sat.	S^{in}	0.60	–
total flux	Q	$1.196\ 10^{-5}$	m/s

5 Approximate numerical solution

5.1 Initial conditions

The preceding theoretical considerations are confirmed by numerical solutions of Eq. (23) with a simple jump-type hysteresis, as formulated in Eq. (29). The initial conditions are monotone and of the form

$$s(z,0) = S^{\mathrm{out}} + (S^{\mathrm{P}} - S^{\mathrm{out}})(1 - \Theta(z - z^*)) \tag{41}$$

where S^{out} is given in Table 1. Note that all initial conditions are monotone and do not have an overshoot. Two cases, labelled A and B, will be illustrated in the figures, namely

A: $S^{\mathrm{P}} = 0.6554 = S^*$ with width $z^* = 0.25$
B: $S^{\mathrm{P}} = 0.9540 \neq S^*$ with width $z^* = 0.015$.

Case A is chosen to illustrate travelling wave solutions with $c_{\mathrm{im}} = c_{\mathrm{dr}}$. The second initial condition illustrates a general overshoot solution with two wave speeds $c_{\mathrm{im}} \neq c_{\mathrm{dr}}$. Moreover it illustrates one possibility for the limit $z^* \to 0$ and $S^{\mathrm{P}} \to 1 - S_{\mathbb{O}\mathrm{r}}{}^{\mathrm{im}}$ in which a very thin saturated layer (that may arise from sprinkling water on top of the column) initiates an overshoot profile. This could provide a partial answer to the question of how saturation overshoot profiles can be initiated.

5.2 Numerical methods

The numerical solution of Eq. (29) was performed using the open source toolkit for computational fluid mechanics Open∇FOAM [82]. This requires to develop an appropriate solver routine. The solver routine employed here was derived from the solver

`scalarTransportFoam` of the toolkit. Two different discretizations of Eq. (29) have been implemented. One is based on a direct discretization of $\partial f_i(S)/\partial z$ using the `fvc::div`-operators, the other on $f_i'(S) \times \partial S/\partial z$ using `fvc::grad`-operators. For the discretization of the time derivatives an implicit Euler scheme was chosen, for the discretization of $\partial S/\partial z$ an explicit least square scheme, and for the discretization of the second order term an implicit Gauss linear corrected scheme has been selected. The second order term had to be regularized by replacing the function $D_i(S)$ with $\max_{S \in [0,1]}\{D_i(S), 10^{-3}\}$. This avoids oscillations at the imbibition front. The discretized system was solved with an incomplete Cholesky conjugate gradient solver in Open∇FOAM. The numerical solutions were found to differ only in the numerical diffusion of the algorithms. The divergence formulation seems to be numerically more stable and accurate.

5.3 Results

Equation (38) can have one solution, several solutions or no solution. This can be seen numerically, but also analytically. Depending on the values of the parameters the velocity of the imbibition front may be larger or smaller than that of the drainage front. With the parameters from Table 1, the overshoot saturation for a travelling wave as computed from (38) is found to be $S^* = 0.6554$ and its velocity is $c_{\mathrm{dr}}(S^*) = c_{\mathrm{im}}(S^*) = 4.2$.

The travelling wave solution expected from the graphical construction in Figs. 1a and b for the initial condition A with $S^{\mathrm{P}} = S^* = 0.6554$ and width $z^* = 0.25$ is displayed in Fig. 1c at the initial time $t = 0$ and after dimensionless time $t = 0.053222$ corresponding to 4450s. It confirms a travelling wave of the form Eq. (36) whose velocity $c^* = 4.2$ agrees perfectly with that predicted from Eq. (38). We have also checked that the solution does not change with grid refinement.

For different initial conditions the numerical solutions also agree with the theoretical considerations. Saturation overshoot is found also when initially a thin saturated layer with steplike or linear profile is present. These solutions, however, do not form travelling waves. Instead they have $c_{\mathrm{im}} \neq c_{\mathrm{dr}}$ for their imbibition and drainage front as predicted analytically. For $S^{\mathrm{P}} > S^*$, the overshoot region grows linearly with time at the rate $c_{\mathrm{im}} - c_{\mathrm{dr}}$. Such an overshoot solution is generated by the second initial condition B and compared with the travelling wave solution in Fig. 2. The non-travelling overshoot for initial condition B with $z^* = 0.015$ and $S^{\mathrm{P}} = 0.954$ is shown as the solid profiles at times $t = 0, 0.02392, 0.053222$ corresponding to $0, 2000, 4450$s. The profile quickly approaches an overshoot solution with plateau value $S \approx 0.682$ close to the saturation of the Welge tangent construction. This is higher than the plateau value $S^* = 0.6554$. The difference will be difficult to observe experimentally because of the large uncertainties in the measurements [54,55]. The velocities of the numerical imbibition and drainage fronts in the case of initial conditions B with $z^* = 0.015$ and $S^{\mathrm{P}} = 0.954$ (solid curves in Fig. 2) again agree perfectly with $c_{\mathrm{im}}(0.682) = 4.27$ and $c_{\mathrm{dr}}(0.682) = 2.813$ from the theoretical analysis.

Other values of the initial saturation S^{P} have also been investigated. A rich phenomenology of possibilities indicates that the existence or nonexistence of overshoot solutions depends very sensitively on the parameters of the problem and the initial conditions.

Note also the asymmetric shape of the overshoot solutions (travelling or not). This asymmetry resembles the asymmetry seen in experiment [54,55]. While the leading imbibition front is steep, the trailing drainage front is more smeared out. This results from the capillary flux term $D_i(S)$ whose values at S^{out} are smaller than at S^{in}.
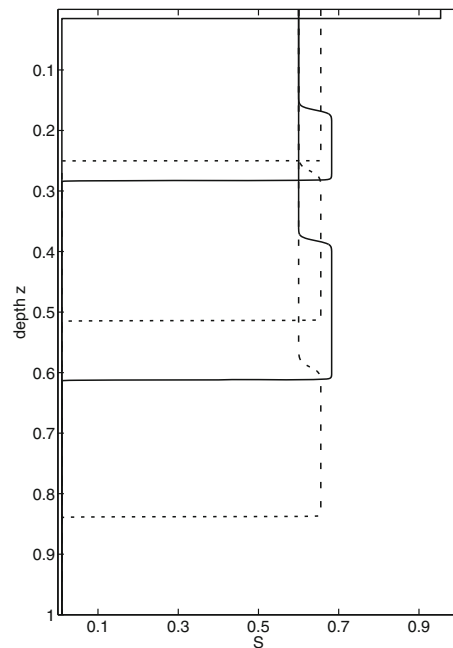
Fig. 2. Numerical solutions $S(z, 0)$, $S(z, 0.02392)$, $S(z, 0.053222)$ of Eq. (29) at dimensionless times $t = 0, 0.02392, 0.053222$ with parameters from Table 1 for initial condition A (dashed) and B (solid). For case A (shown as a short dashed line) the profile for $t = 0.053222$ is the same as in Fig. 1c. For the solid profiles (case B) the imbibition front moves with speed $c_{im} = 4.27$ while the trailing drainage front moves with $c_{dr} = 2.813$.

6 Critical perspective and challenges

Theoretical analysis and the numerical results suggest, that propagation of travelling and non-travelling saturation overshoots must be expected in the traditional setting for hysteretic relative permeability functions of jump-type. Although hysteresis in the relative permeabilities may be small, the hysteresis in the flux functions can be significant and the saturation overshoot can be pronounced depending on the parameters. Note, that hysteresis in P_c is not needed to obtain propagation of the overshoot.

At first glance this situation seems to be at variance with mathematical proofs of the unconditional stability of the traditional theory [11,57,58,61,68] where it is argued that saturation overshoot is impossible with or without capillary hysteresis. Note however, that the mathematical proofs are based on the elliptic–parabolic Richards Eq. (19). Analytical arguments and numerical solutions seem to show that overshoot saturations (travelling or non-travelling) are possible in the more general case of Eq. (17) with hysteresis of jump-type in the relative permeabilities. Thus, failure to reproduce saturation overshoot cannot be considered a valid criticism of the established traditional theory. More theoretical and analytical work is needed to clarify the situation and the crossover between these regimes.

Extensive numerical solutions of Eq. (29) reveal a strong dependence on the initial conditions. This could provide partial answers to the question how saturation overshoot can be initiated. It suggests also that the experimental observations of saturation overshoot could be largely explained as a consequence of hysteresis in the relative permeability and fractional flow functions. There are, however, numerous other experimental phenomena (related to the residual, irreducible and trapped

phase fractions) that cannot be adequately predicted by the traditional model with hysteresis [24,41,46,47,49,50].

The current situation with respect to saturation overshoot is still unsatisfactory in several respects and poses a number of challenges for future research. Experimentally, the assumption of travelling waves [55,62], i.e. the assumption $c_{im} = c_{dr}$, has to be the best of our knowledge, not been clearly demonstrated [54]. The uncertainties in saturation measurement and the relatively short columns make it difficult to establish that the two fronts move at the same speed. Theoretically, the existence of overshoot solutions needs more rigorous analysis, especially in higher dimensions. Also the relation with front stability and fingering poses challenges for theory and experiment.

References

1. R. Hilfer, Adv. Chem. Phys. **XCII**, 299 (1996)
2. M. Muskat, The Flow of Homogeneous Fluids Through Porous Media (McGraw Hill, New York, 1937)
3. A.E. Scheidegger, The Physics of Flow Through Porous Media (University of Toronto Press, Canada, 1957)
4. R.E. Collins, Flow of Fluids Through Porous Materials (Reinhold Publishing Co., New York, 1961)
5. J. Bear, Dynamics of Fluids in Porous Media (Elsevier Publ. Co., New York, 1972)
6. G.D. Marsily, Quantitative Hydrogeology – Groundwater Hydrology for Engineers (Academic Press, San Diego, 1986)
7. G.P. Willhite, Waterflooding, series SPE Textbook Series, Vol. 3 (Society of Petroleum Engineers, USA, 1986)
8. L.W. Lake, Enhanced Oil Recovery (Prentice Hall, Englewood Cliffs, 1989)
9. F.A.L. Dullien, Porous Media – Fluid Transport and Pore Structure (Academic Press, San Diego, 1992)
10. M. Sahimi, Flow and Transport in Porous Media and Fractured Rock (VCH Verlagsgesellschaft mbH, Weinheim, 1995)
11. M. Eliassi, R.J. Water Resour. Res. **37**, 2019 (2001)
12. M.I.J. van Dijke, K. Sorbie, Phys. Rev. E **66**, 046302 (2002)
13. I. Fatt, AIME Petrol. Trans. **207**, 144 (1956)
14. M.M. Dias, A.C. Payatakes, J. Fluid Mech. **164**, 305 (1986)
15. M. Blunt, P. King, Phys. Rev. A **42**, 4780 (1990)
16. M. Blunt, M.J. King, H. Scher, Phys. Rev. A **46**, 7680 (1992)
17. M. Ferer, G.S. Bromhal, D.H. Smith, Phys. Rev. E **67**, 051601 (2003)
18. R. Hilfer, H. Besserer, "Old problems and new solutions for multiphase flow in porous media", in *Porous Media: Physics, Models, Simulation*, edited by A. Dmitrievsky, M. Panfilov (World Scientific Publ. Co., Singapore, 2000), p. 133
19. E. Buckingham, "Studies on the movement of soil moisture," Tech. Rep. (U.S. Department of Agriculture, Bureau of Soils, 1907)
20. L.A. Richards, Physics **1**, 318 (1931)
21. R.D. Wyckoff, H. Botset, Physics **7**, 325 (1936)
22. M. Muskat, M. Meres, Physics, **7**, 346 (1936)
23. M. Leverett, Trans. AIME **142**, 152 (1941)
24. R. Hilfer, Phys. Rev. E **73**, 016307 (2006)
25. R. Hilfer, R. Helmig, Adv. Water Res. **27**, 1033 (2004)
26. W.O. Smith, P.D. Foote, P.F. Busang, Physics **1**, 18 (1931)
27. S. Buckley, M. Leverett, Trans. AIME **146**, 107 (1942)

28. J. Challis, Phil. Mag. Ser. 3, **32**, 494 (1848)
29. G. Stokes, Phil. Mag. Ser. 3, **33**, 349 (1848)
30. P. Lax , Comm. Pure Appl. Math. **7**, 159 (1954)
31. P. LeFloch, Hyperbolic Systems of Conservation Laws (Birkhäuser, 2002)
32. H. Alt, S. Luckhaus, A. Visintin, Ann. Mat. Pura Appl. **136**, 303–316 (1984)
33. K. Aziz, A. Settari, Petroleum Reservoir Simulation (Applied Science Publishers Ltd., London, 1979)
34. R. Helmig, Multiphase Flow and Transport Processes in the Subsurface (Springer, Berlin, 1997)
35. Z. Chen, G. Huan, Y. Ma, Computational Methods for Multiphase Flow in Porous Media (SIAM, 2006)
36. B. Biswal, P.E. Øren, R.J. Held, S. Bakke, R. Hilfer, Image Anal. Stereol. **28**, 23 (2009)
37. L. Anton, R. Hilfer, Phys. Rev. E **59**, 6819 (1999)
38. R. Hilfer, H. Besserer, Physica B **279**, 125 (2000)
39. R. Hilfer, Physica A **359**, 119 (2006)
40. E. Gerolymatou, I. Vardoulakis, R. Hilfer, J. Phys. D **39**, 4104 (2006)
41. R. Hilfer, Physica A **371**, 209 (2006)
42. S. Manthey, M. Hassanizadeh, R. Helmig, R. Hilfer, Adv. Water Res. **31**, 1137 (2008)
43. R. Hilfer, *Modeling and simulation of macrocapillarity*, in *CP1091, Modeling and Simulation of Materials*, edited by P. Garrido, P. Hurtado, J. Marro (American Institute of Physics, New York, 2009), p. 141
44. R. Hilfer, F. Doster, Transp. Porous Med. **82**, 507 (2010)
45. F. Doster, P. Zegeling, R. Hilfer, Phys. Rev. E **81**, 036307 (2010)
46. F. Doster, R. Hilfer, New J. Phys. **13**, 123030 (2011)
47. F. Doster, O. Hönig, R. Hilfer, Phys. Rev. E **86**, 016317 (2012)
48. R. Hilfer, F. Doster, P. Zegeling, Vadose Zone J. **11**, vzj2012.0021 (2012)
49. O. Hönig, F. Doster, R. Hilfer, Transp. Porous Med., 196 (2013)
50. F. Doster, R. Hilfer, Water Resour. Res. **50**, 1 (2014)
51. E.G. Youngs, Soil Sci. **86**, 202–207 (1958)
52. J. Briggs, D. Katz, "Drainage of water from sand in developing aquifer storage (1966), paper SPE1501 presented 1966 at the 41st Annual Fall Meeting of the SPE, Dallas, USA
53. R. Glass, T. Steenhuis ad J. Parlange, Soil Sci. **148**, 60 (1989)
54. S. Shiozawa, H. Fujimaki, Water Resour. Res. **40**, W07404 (2004)
55. D. DiCarlo, Water Resour. Res. **40**, W04215 (2004)
56. J.L. Nieber, Geoderma **70**, 207 (1996)
57. F. Otto, J. Diff. Eq. **131**, 20 (1996)
58. F. Otto, Adv. Math. Sci. Appl. **7**, 537 (1997)
59. S. Geiger, D. Durnford, Soil Sci. Soc. Am. J. **64**, 460 (2000)
60. M. Eliassi, R.J. Glass, Water Resour. Res. **38**, 1234 (2002)
61. A. Egorov, R. Dautov, J. Nieber, A. Sheshukov, Water Resour. Res. **39**, 1266 (2003)
62. D. DiCarlo, Adv. Water Res. **28**, 1021 (2005)
63. C. van Duijn, L. Peletier, I. Pop, SIAM J. Math. Anal. **39**, 507 (2007)
64. L. Cueto-Felgueroso, R. Juanes, Phys. Rev. Lett. **101**, 244504 (2008)
65. L. Cueto-Felgueroso, R. Juanes, Phys. Rev. E **79**, 036301 (2009)
66. D. diCarlo, Water Resour. Res. **49**, 4531 (2013)
67. H. Alt, S. Luckhaus, Math. Z. **183**, 311 (1983)
68. T. Fürst, R. Vodak, M. Sir, M. Bil, Water Resour. Res. **45**, W03408 (2009)
69. D. DiCarlo, M. Mirzaei, B. Aminzadeh, H. Dehghanpur, Transp. Porous Med. **91**, 955 (2012)
70. Y. Xiong, J. Hydrology **510**, 353 (2014)
71. J. Nieber, R. Dautov, E. Egorov, A. Sheshukov, Transp. Porous Med. **58**, 147 (2005)
72. C. van Duijn, Y. Fan, L. Peletier, I. Pop, Nonlinear Anal. Real World Appl. **14**, 1361 (2013)
73. T. Bauters, D. DiCarlo, T. Steenhuis, Y. Parlange, J. Hydrology **231-232**, 244 (2000)

74. M. Deinert, J. Parlange, K. Cady, T. Steenhuis, J. Selker, Water Resour. Res. **39**, 1263 (2003)
75. S. Bottero, M. Hassanizadeh, P. Kleingeld, T. Heimorvaara, Water Resour. Res. **47**, W10505 (2011)
76. R. Hilfer, P.E. Øren, Transp. Porous Med. **22**, 53 (1996)
77. Y. Mualem, Water Resour. Res. **10**, 514 (1974)
78. J.C. Parker, R.J. Lenhard, Water Resour. Res. **23**, 2187 (1987)
79. R. Lenhard, J. Parker, Water Resour. Res. **23**, 2197 (1987)
80. M.T.v. Genuchten, Soil Sci. Soc. Am. J. **44**, 892 (1980)
81. L. Luckner, M.T.v. Genuchten, D. Nielsen, Water Resour. Res. **25**, 2187 (1989)
82. `http://www.openfoam.com/`